

Accepted Manuscript

Nano-targeted relaxin impairs fibrosis and tumor growth in pancreatic cancer and improves the efficacy of gemcitabine in vivo

Deby F. Mardhian, Gert Storm, Ruchi Bansal, Jai Prakash



PII: S0168-3659(18)30570-4
DOI: doi:[10.1016/j.jconrel.2018.09.031](https://doi.org/10.1016/j.jconrel.2018.09.031)
Reference: COREL 9483

To appear in: *Journal of Controlled Release*

Received date: 7 June 2018
Revised date: 11 September 2018
Accepted date: 30 September 2018

Please cite this article as: Deby F. Mardhian, Gert Storm, Ruchi Bansal, Jai Prakash , Nano-targeted relaxin impairs fibrosis and tumor growth in pancreatic cancer and improves the efficacy of gemcitabine in vivo. Corel (2018), doi:[10.1016/j.jconrel.2018.09.031](https://doi.org/10.1016/j.jconrel.2018.09.031)

This is a PDF file of an unedited manuscript that has been accepted for publication. As a service to our customers we are providing this early version of the manuscript. The manuscript will undergo copyediting, typesetting, and review of the resulting proof before it is published in its final form. Please note that during the production process errors may be discovered which could affect the content, and all legal disclaimers that apply to the journal pertain.

Nano-targeted relaxin impairs fibrosis and tumor growth in pancreatic cancer and improves the efficacy of gemcitabine *in vivo*

Deby F. Mardhian^a, Gert Storm^{a,b}, Ruchi Bansal^{a,*}, Jai Prakash^{a,c*,§}

^aSection - Targeted Therapeutics, Department of Biomaterials Science and Technology, Faculty of Science and technology, University of Twente, Enschede, The Netherlands. ^bDepartment of Pharmaceutics, Utrecht University, Utrecht, The Netherlands. ^cScarTec Therapeutics BV, Enschede, The Netherlands.

*Authors contributed equally to this work

§Corresponding author's email: j.prakash@utwente.nl

Corresponding postal address:

Section - Targeted Therapeutics
Department of Biomaterials Science and Technology
Faculty of Science and Technology
University of Twente
Zuidhorst 254
7500 AE Enschede
The Netherlands
T (+31)-53-489 3096

Abbreviations:

Human pancreatic stellate cells (hPSCs), cancer-associated fibroblasts (CAFs), pancreatic ductal adenocarcinoma (PDAC), Relaxin-2 (RLX), superparamagnetic iron oxide nanoparticles (SPION), gemcitabine (Gem), transforming growth factor β (TGF- β), extracellular matrix (ECM), α -smooth muscle actin (α -SMA), collagen-I (Col-I), Conditioned Medium (CM)

Abstract

Cancer-associated fibroblasts (CAFs), are the key effector cells in pancreatic ductal adenocarcinoma (PDAC), known to induce tumor growth and progression. Pancreatic stellate cells (PSCs) are the precursors of CAFs in PDAC that secrete abundant extracellular matrix, growth factors and cytokines. In this study, we targeted human relaxin-2 (RLX), an endogenous hormone, to PSCs to inhibit their differentiation into CAF-like myofibroblasts. RLX significantly inhibited TGF- β induced PSCs differentiation by inhibiting pSmad2 signaling pathway. *In vitro* in primary human PSCs (hPSCs), treatment with RLX dose-dependently inhibited the migration, contraction, and protein expression of alpha smooth muscle actin and collagen I. These data demonstrate that RLX can regulate hPSCs activation *in vitro*. However, RLX has several drawbacks i.e. poor pharmacokinetics and systemic vasodilation, that limits its preclinical and clinical application. Thus, we designed and successfully synthesized a nanoparticle system by chemically conjugating RLX to superparamagnetic iron oxide nanoparticle (SPION) to improve its pharmacokinetics. Interestingly, we found RLX-SPION to be more efficacious compared to free RLX *in vitro*. Significantly, we observed RLX-SPION retarded the tumor growth by itself and also potentiated the effect of gemcitabine in a subcutaneous co-injection (Panc1 and hPSCs) tumor model. The treatment resulted in significant inhibition in tumor growth, which was attributed to reduced collagen I (ECM), desmin (hPSC marker) and CD31 (endothelial marker) expression. In contrast, free RLX showed no significant effects. Altogether, this study presents a novel therapeutic approach against tumor stroma using RLX-SPION to achieve an effective treatment against pancreatic tumor.

Keywords: Relaxin-2, superparamagnetic iron-oxide nanoparticles, pancreatic stellate cells, cancer-associated fibroblasts, pancreatic cancer, tumor stroma.

1. Introduction

Pancreatic cancer is one of the most deadly malignancies with a 5-year survival rate only of 8% [1]. Annually, more than 50,000 people in U.S. and 90,000 people in Europe are diagnosed with pancreatic ductal adenocarcinoma (PDAC), the most common form of pancreatic cancer [1]. Most of the cases of pancreatic cancer are diagnosed in advanced stage, making the surgical treatment not feasible, and radiotherapy and chemotherapy remains the golden standard [2,3]. However, these treatments only benefit for few months [4,5]. One of the reasons for the treatment failure is the abundant desmoplastic reaction or so-called tumor stroma that accounts for around 90% of the tumor, which acts as a barrier to chemotherapy [6,7]. Tumor stroma contains different cell types including cancer-associated fibroblasts (CAFs), endothelial cells, pericytes, macrophages and other immune cells. CAFs are the most prominent stromal cells that produce abundant extracellular matrix (ECM) and secrete several growth factors which in turn activate tumor cells resulting in tumor progression and metastasis [8,9]. In addition, the rapid tumor cell growth in a limited area imposes solid stress and high cellular density, limiting the diffusion of chemotherapeutic drugs [7]. In literature, modulation of tumor stroma is proposed as a potential therapeutic approach to enhance the effect of chemotherapy [8,10,11].

Pancreatic stellate cells (PSCs) are believed to be the main source of cancer-associated fibroblasts (CAFs) and therefore becoming an promising target for modulating tumor stroma [12,13]. In PDAC, PSCs acquire activated phenotype which is associated with high proliferative and secretive phenotype compared to quiescent PSCs. Excessive secretion of ECM by the activated PSCs leads to tumor-associated fibrosis which presents a stromal barrier for drug penetration [14]. Therefore, we hypothesized that inhibition of PSC activation might be an interesting approach to potentiate the effect of chemotherapy for the treatment of pancreatic cancer.

Relaxin and relaxin-like peptides are the part of the insulin superfamily that is present in all mammals and have diverse functions in both male and female reproduction. Also they act as neuropeptide in nervous system, as vasodilator and cardiac stimulant in cardiovascular system, and as anti-fibrotic agents [15]. Humans and primates as higher mammals have both relaxin-1 and relaxin-2 (RLX), while other mammals have only RLX1 [15]. It was first recognized as a substance that function to relax the pelvic ligament and influence female reproductive tract [16]. In humans, relaxin is produced in corpus luteum during pregnancy and the decidua in females while in males it is produced in the prostate [17]. Other than its function in reproductive organs, studies have demonstrated that exogenous relaxin-2 (RLX) plays a number of significant roles, which contribute to its therapeutic potential. Previous studies have shown the efficacy of RLX in reducing fibrosis [18–22]. Relaxin-2 function by binding to its cognate receptor, high affinity leucine-rich containing G-protein-coupled receptor LGR7 or now known as RXFP1 (relaxin family peptide receptor type 1) to resolve fibrosis by inhibiting Smad2/3 phosphorylation and stimulating MMPs production [15]. However, direct application of RLX is limited due to its relatively small size (6 kDa), short circulation half-life, and undesired effect such as systemic vasodilation.

The delivery of anticancer therapeutics into tumor by employing nanoparticles has made significant progress. The encapsulation of therapeutics into nanoparticles or conjugation to nanoparticles

represent promising strategies to address several problems such as poor solubility, limited stability, rapid metabolism and undesired side effects [23,24]. For biological applications, nanoparticles need to be biocompatible, non-toxic, and stable at physiological pH. Superparamagnetic iron oxide nanoparticles (SPION) are one of the developed systems in the cancer management due to its high biocompatibility. In the body, when the SPION are exposed to oxygen, they are converted to maghemite ($\gamma\text{-Fe}_2\text{O}_3$), metabolized and transported by proteins like ferritin, transferritin, and hemosiderin [25]. SPION also have the ability to conjugate with a range of ligands, functional groups, and drugs for receptor-specific targeting, improved drug delivery efficiency [26], and the ability to respond to stimuli such as magnetic field and heat [25,27].

Considering the anti-fibrotic effect of RLX and the diverse applications of SPION, in this study, we hypothesized that delivering RLX using SPION could be an interesting approach to inhibit the differentiation of human PSCs (hPSCs) into CAF-like myofibroblasts and thereby impair tumor-promoting effects *in vivo*. We showed that RLX receptor RXFP1 was overexpressed in activated hPSCs. We first examined the inhibitory effect of RLX on hPSCs differentiation, migration and contraction *in vitro*. Then, we designed and prepared delivery system by conjugating RLX on the surface of SPION using biochemical conjugation techniques. Next, we compared the effect of the RLX-SPION and free RLX *in vitro*. Then, we examined whether RLX-SPION inhibits hPSCs *in vivo* and thereby reduce the tumor growth in a stroma-rich co-injection pancreatic tumor xenograft model. In addition, we also evaluated whether co-treatment of RLX-SPION is able to induce the effect of chemotherapy i.e. gemcitabine.

2. Materials and methods:

2.1 Cells

Primary human pancreatic stellate cells (ScienCell, Carlsbad, USA) were cultured in complete Stellate Cell medium (supplemented with 1% Stellate Cell Growth Supplements (SteCGS), 1% penicillin/streptomycin, and 2% FBS) (ScienCell). Panc-1 cancer cells were cultured in Dulbecco's Modified Eagles Medium (DMEM) high glucose (4.5 g/l) with L-glutamine (GE Healthcare, Vienna, Austria) supplemented with 100 $\mu\text{g/ml}$ penicillin/streptomycin (Sigma Aldrich, St. Louis, MO, USA), and 10% FBS (Lonza, Verviers, Belgium). Cells were maintained at 37 °C in a humidified 5% CO_2 atmosphere.

2.2 Quantitative real time PCR

To examine the expression of relaxin receptor RXFP1 on TGF- β induced hPSCs differentiation, cells were seeded into a 12 well plate at a seeding density of 50,000 cells/well. The next day, cells were starved for 24 hours, then treated with TGF- β (5 ng/ml, Roche, Mannheim, Germany). After 24 hours, total RNA was isolated using GenElute™ Mammalian Total RNA Miniprep Kit (Sigma Aldrich) and the RNA concentration was measured using a NanoDrop® ND-1000 Spectrophotometer (Thermo Scientific, Rockford, IL, USA). cDNA was synthesized with iScript™ cDNA Synthesis Kit (BioRad, Veenendaal, The Netherlands), and 10 ng cDNA were used for each PCR reaction. The real-time PCR primers (Table 1) were purchased from Sigma Aldrich. Quantitative real time PCR was performed with

2x SensiMix SYBR and Fluorescein Kit (Bioline GmbH, Luckenwalde, Germany) using a BioRad CFX384 Real-Time PCR detection system (BioRad). Gene expression levels were normalized to the expression of the house-keeping gene 18s rRNA.

Table 1 Sequences of forward and reverse primers used during real-time PCR.

Gene	Forward Primer	Reverse Primer
r18s rRNA	TGAGGTGGAACGTGTGATCA	CCTCTATGGGCCCCGAATCTT
α -SMA	CCCCATCTATGAGGGCTATG	CAGTGGCCATCTCATTTTCA
Collagen I	GTACTGGATTGACCCCAACC	CGCCATACTCGAACTGGAAT
Fibronectin	GTATACGAGGGCCAGCTCAT	CCCAGGAGACCACAAAGCTA
RXFP1	AGTCTCTCAGCCTAGAAGGGA	TACAGCTGCGAACATGTGGT

2.3 F-actin staining

To analyse the effect of RLX on the F-actin organization of TGF- β -induced hPSCs differentiation, cells were seeded into 24 well plate at a seeding density of 4,000 cells/well and starved for 24 hours. hPSCs were then incubated with 250 ng/ml RLN and/or 5 ng/ml TGF- β for 24 hours and then washed three times with PBS and fixed in 4% formaldehyde (Sigma Aldrich) in PBS for 20 minutes. After permeabilizing the cells with 0.1 M Triton X-100 (Sigma Aldrich) for 5 minutes, F-actin was stained with phalloidin (Life Technologies, Gaithersburg, MD, USA) at concentration of 250 ng/ml for 60 minutes. Next, cells were washed with PBS and then covered with DAPI-containing mounting medium (Sigma). Images were made using an EVOS FI fluorescent microscope (Life Technologies) at ex. 540 nm/em 565 nm.

2.4 Relaxin conjugation to SPION

The conjugation of RLX to SPION was performed chemically using EDC/NHS reaction. One hundred microliter SPION (Micromod, Rostock, Germany) at concentration 5 mg/ml were added with 50 μ l mixture of 5 μ M EDC and 17.4 μ M NHS dissolved in MES buffer (pH 6.3). After 45 minutes of incubation, the SPION were washed with PBS and spun down in a 30 kDa amicon column at 5,000 RPM (3 times) to remove excess EDC and NHS. Eventually, the activated SPION were incubated with 5 μ g RLX overnight at 4 °C. The next day, the reaction was stopped by washing with PBS (3 times) in amicon column. Supernatant of first washing was collected for dot blot analysis. To deactivate the remaining carboxylic group on the SPION, particles were incubated with 10 μ g glycine for 30 minutes at room temperature. The recovered RLX-SPION were washed with PBS (3 times) in amicon columns and resuspended in 100 μ l PBS.

2.5 Dot blot

To evaluate the yield of conjugation, 5 μ l of RLX, SPION, RLX-SPION, and supernatant at different dilution were spotted on nitrocellulose membrane and allowed to dry for 10 minutes. The membrane was then incubated in 5% non-fat dry milk dissolved in TBST-20. After 1 hour incubation, the membrane was washed with TBST-20 (3 times), followed by incubation with anti-RLX primary antibody and species specific horseradish peroxidase (HRP) labelled secondary and tertiary antibody. RLX was

detected with Pierce™ ECL Plus Western Blotting substrate kit (Thermo Scientific) and the membranes were exposed to FluorChem™ M System (ProteinSimple, San Jose, USA).

2.6 Prussian blue staining

To ensure the recovery of nanoparticles, 5 µl of RLX, SPION, RLX-SPION, and supernatant at different dilution were spotted on nitrocellulose membrane and allowed to dry for 10 minutes. Iron oxide was detected with Prussian Blue staining kit (Sigma Aldrich). Images were captured using normal camera.

2.7 Western blot

To evaluate the effect of RLX on the expression of hPSCs activation markers α -SMA and collagen-1, hPSCs were seeded into a 12 well plate at seeding density 40,000 cells/well. Next day, the medium was changed with 0% FBS Stellate Cell medium to starve hPSCs for 24 hours. Subsequently, hPSCs were incubated with 5 ng/ml TGF- β and RLX at different concentration for 24 hours. To evaluate the effect of RLX on TGF- β mediated phosphorylation of Smad2 in hPSCs, cells were seeded into a 12 well plate at a seeding density 40,000 cells/well. The cells were starved for 24 hours the next day and treated with 5 ng/ml TGF- β and RLX at different concentration for 1 hour. To examine the effect of RLX-SPION, hPSCs were seeded and starved for 24 hours. The cells were then treated with SPION, RLX, or RLX-SPION for 24 hours to examine the effect on protein expression of α -SMA and collagen-1 (1 hour for Smad2 phosphorylation). Cells were lysed using 1x blue loading buffer containing 1x DTT reducing agent (Cell Signaling Technology, Leiden, the Netherlands) and homogenized using ultrasonication. Lysates were collected for Western blot analysis. Protein lysates were separated on a 10% Tris-Glycine gel (Thermo Scientific) and then transferred onto a PVDF membrane (Thermo Scientific). The blots were incubated with the required primary antibody overnight at 4 °C followed by incubations with species specific HRP conjugated secondary and tertiary antibody for 1 hour at room temperature. Antibodies details are given in Table 2. Proteins were detected with Pierce™ ECL Plus Western Blotting substrate kit (Thermo Scientific) and the membranes were exposed to FluorChem™ M System (ProteinSimple, San Jose, USA). The protein signals were quantified using ImageJ Software (NIH, MD) and normalized to β -actin.

2.8 Cell proliferation

hPSCs were seeded into a 96 well plate at a seeding density of 4,000 cells/well. The next day, cells were starved for 24 hours and treated with RLX at different concentration for another 24 hours. Number of cell was observed using alamar blue assay (Invitrogen, Carlsbad, USA). In each well, mixture of 10 µl of alamar blue dye and 90 µl of hPSC growth media was added. After 4 hours, fluorescent signal was measured using a VIKTOR™ plate reader (Perkin Elmer, Waltham, Massachusetts).

2.9 Scratch assay

To evaluate the effect of RLN on hPSCs migration, cells were seeded in a 24 well plate at a seeding density of 60,000 cells/well and starved for 24 hours.. After starvation, a scratch was made on the culture plate using a 200 µl pipette tip fixed in a custom-made holder. Cells were washed with serum-

free media and incubated with serum-free media and RLX at different concentrations. The same treatment was applied for the evaluation of RLX-SPION effect on hPSCs migration. Images were captured at $t = 0$ h and $t = 7$ h using an EVOS microscope. Images were analyzed using ImageJ software to quantitate the area of the scratch and represented as percentage of wound closure.

2.10 Animal study

Six-week old male CB17 SCID mice (Janvier Labs, Le Genest-Saint-Isle, France) were subcutaneously injected with a 1:2 mixture of 1.5×10^6 Panc-1 and 3×10^6 hPSCs. Tumor sizes were assessed twice a week. Tumor volumes were calculated using a standard formula (volume = length \times width² \times 0.5). The treatments were started at day 10 when tumors were established. Mice were injected intravenously with vehicle, RLX, or RLX-SPION with/without gemcitabine (50mg/kg, intraperitoneally). At the end of the experiment, animals were euthanized, tumors were harvested and snap frozen in cold 2-methyl butane (Fisher Scientific). Frozen tumors were stored at -80°C until analysis.

2.11 Immunohistochemical Staining of mouse tumors

Mouse tumors were embedded in Cryomatrix (Thermo Scientific) and stored at -80°C . Tumors were cut into 7 μm thick sections using Cryotome FSE (Thermo Scientific), dried and fixed in acetone for 15 minutes. Tumor sections were rehydrated in PBS for 10 minutes then incubated with primary antibody diluted in PBS overnight at 4°C . Antibodies details are given in Table 2. The next day, slides were washed 3 times with PBS before incubation with secondary HRP-labeled antibody diluted in PBS supplemented with 5% vol of normal mouse serum. Staining with HRP-labeled secondary antibodies was continued as described elsewhere [28]. Images have been made using a Hamamatsu NanoZoomer Digital slide scanner 2.0HT (Hamamatsu Photonics, New Jersey, USA).

Table 2. Details of the antibodies used in the study

Antibody	Source	Dilution	
		Blotting	IHC
Mouse monoclonal anti-actin, α -smooth muscle	Sigma Aldrich	1:500	
Goat anti-type I collagen	Southern Biotech	1:250	1:250
Rabbit monoclonal anti-Phospho-Smad2/3	Cell Signaling	1:1000	
Rabbit monoclonal anti-Smad2/3	Cell Signaling	1:1000	
Goat polyclonal IgG anti-desmin	Santa Cruz		1:250
Rat anti-mouse CD31	Southern Biotech		1:100
Rat monoclonal anti-human relaxin-2	RnD System	1:250	
Polyclonal rabbit anti-goat immunoglobulin HRP	Dako	1:2000	1:200
Polyclonal rabbit anti-mouse immunoglobulin HRP	Dako	1:2000	1:200
Polyclonal rabbit anti-rat immunoglobulin HRP	Dako	1:2000	1:200
Polyclonal goat anti-rabbit immunoglobulin HRP	Dako	1:2000	1:200

2.12 Graphs and statistical analyses

All graphs were made using GraphPad Prism version 5.02 (GraphPad Software Inc., San Diego, CA). All values are expressed as a mean \pm standard error of the mean (SEM). Statistical significance of the

results was performed by a two-tailed unpaired student's t-test for comparison of two treatment groups. Differences were considered significant for a p-value of * $p < 0.05$, ** $p < 0.01$, *** $p < 0.001$.

3. Results

3.1 RLX receptor (RXFP1) expression is induced in TGF- β differentiated hPSCs

RLX exerts its effects in hPSCs by binding to extracellular domain of the relaxin family peptide receptor 1 (RXFP1). The gene expression levels of RXFP1 were analyzed in non-activated quiescent hPSCs and TGF- β -activated hPSCs. The activation and differentiation of hPSCs upon TGF- β incubation was confirmed by the morphological changes i.e. stretched and elongated shape, as shown with f-actin staining (Fig. 1A) and hPSC activation markers such as alpha smooth muscle actin (α -SMA), collagen I (Col-1 α 1), and fibronectin (FN) (Figure 1B). Interestingly, we found that the expression of RXFP1 was induced by about 3-fold ($p < 0.001$) after TGF- β activation compared to the non-activated cells as shown in Fig. 1B. These data clearly demonstrate that TGF β activated hPSCs overexpress RXFP1 receptor, suggesting it as an appropriate target.

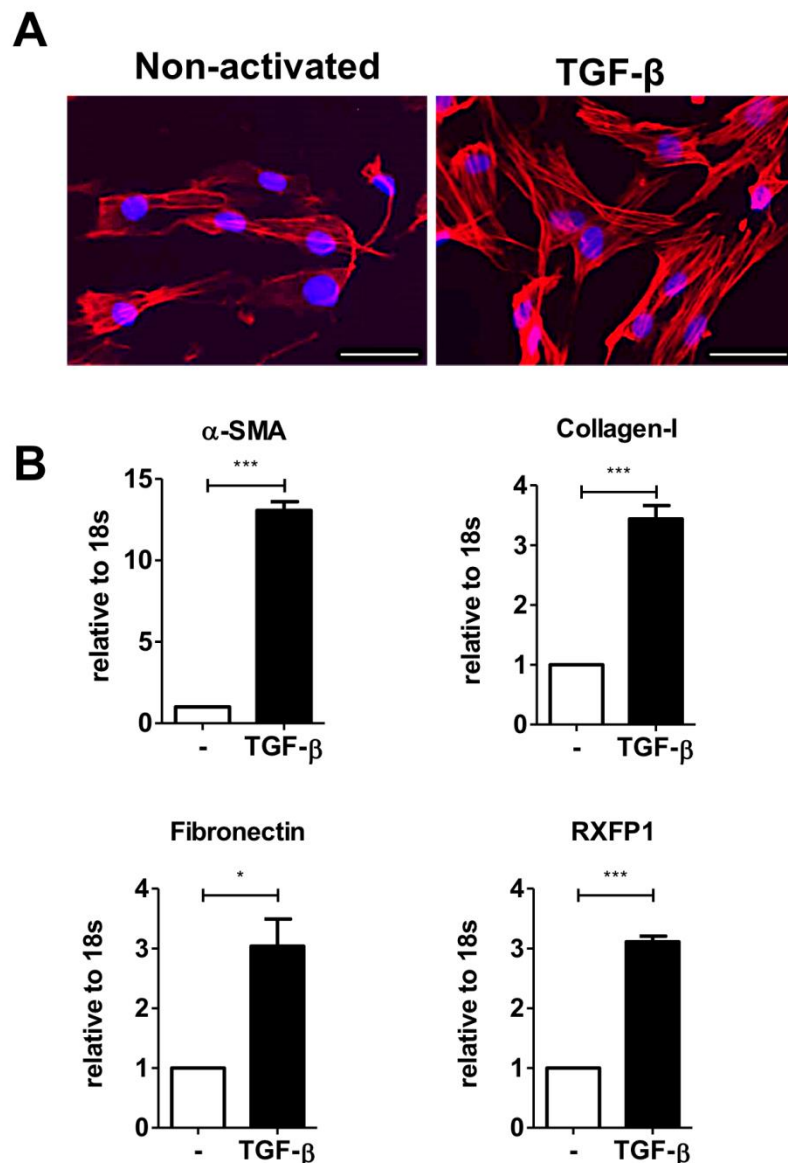


Figure 1. hPSCs differentiation and the expression of the human Relaxin-2 (RLX) specific surface receptor RXFP1 on hPSCs. (A) F-actin staining showing the morphological difference between untreated hPSCs and hPSCs treated with TGF- β for 24 hours. Scale bar 100 μ m. (B) The gene expression of CAF-like myofibroblasts markers α -SMA, Col-1 α 1 (collagen-1), and fibronectin, and RLX receptor RXFP1 in untreated hPSCs and hPSCs treated with TGF- β for 24 hours. Data represents mean \pm SEM for at least 3 independent experiments. Statistical differences are * p <0.05, *** p <0.001

3.2 RLX inhibits TGF- β induced hPSCs differentiation by inhibiting pSmad2 pathway

To examine the effect of RLX on the differentiation of hPSCs, we treated the cells with different concentrations of RLX with TGF- β . We found that RLX inhibited the TGF- β -induced expression of α -SMA and collagen-I in a concentration dependent manner, as shown with the western blot analysis in Fig. 2A. To evaluate whether RLX inhibits the downstream signaling of TGF- β i.e. the phosphorylation of Smad2, we examined the protein expression of pSmad2 compared to total Smad2. The western blot data showed a significant inhibition of TGF β -induced pSmad2/Smad2 ratio by RLX in a concentration-dependent manner, as shown in Fig. 2B.

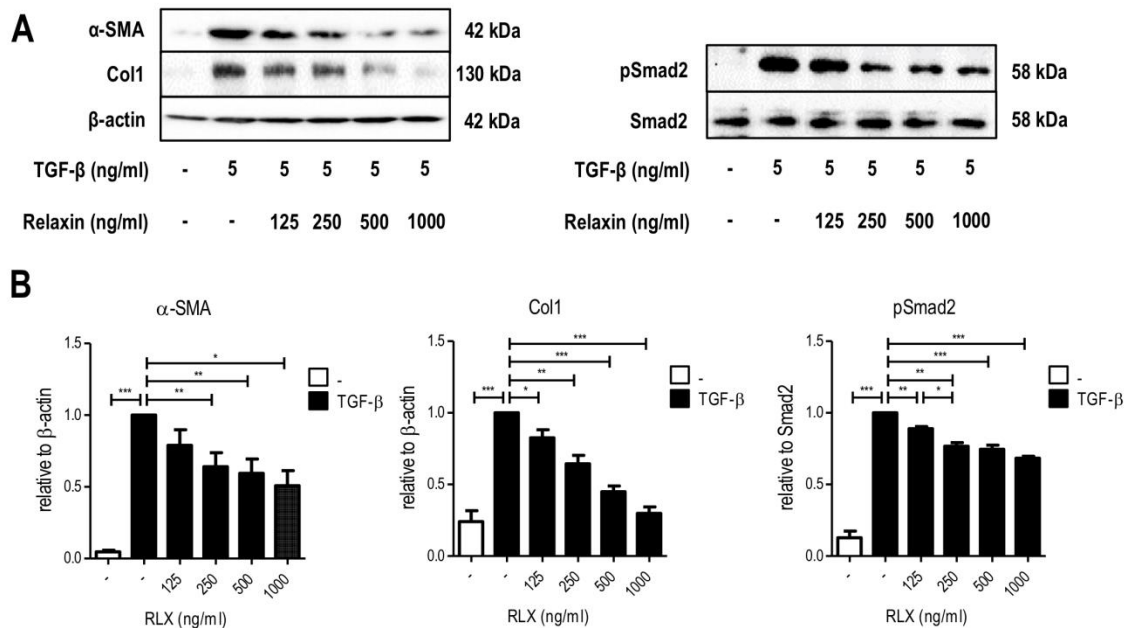


Figure 2. Effect of RLX on TGF- β mediated hPSC differentiation. Western blot (A) and quantification (B) showing the inhibitory effect of RLX (125, 250, 500, 1000 ng/ml) on the protein expression of α -SMA and Col-1 in hPSCs activated with TGF- β for 24 hours compared to untreated hPSCs and the inhibitory effect of RLX (125, 250, 500, 1000 ng/ml) on the phosphorylation of Smad2 in hPSCs activated with TGF- β for 1 hour compared to untreated hPSCs. Protein levels are normalized to β -actin. Data represents mean \pm SEM for at least 3 independent experiments. Statistical differences are * p <0.05, ** p <0.01, *** p <0.001

The inhibition of hPSC activation not only resulted in reduced cytoskeleton marker (α -SMA) and ECM production (collagen-1), but also reduced the TGF- β -induced contractility of hPSCs, as shown with 3D collagen gel contraction assay (Fig. 3A). In addition, we evaluated the effect of RLX on the migration of hPSCs using scratch assay. We found that TGF- β did not induce the migration of hPSCs (data not shown), which is line of the previous study [14]. Yet, RLX treatment resulted in a significant inhibition in cell migration compared to control (untreated) cells (Figure 3B). These data show that RLX is able to counteract the effect of TGF- β directly which leads to the inhibition of TGF- β -induced differentiation and contraction as well as migration of hPSCs.

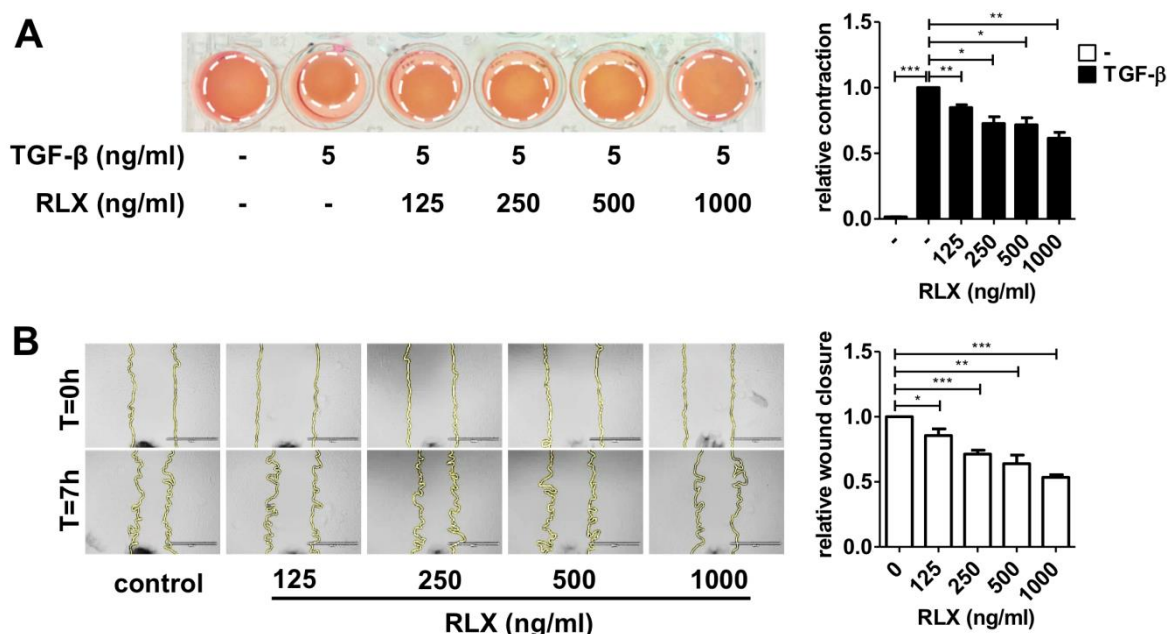


Figure 3. Effect of RLX on hPSC contractility and migration. Representative images and quantification showing the effect of RLX (125, 250, 500, 1000 ng/ml) on the contraction of hPSCs activated with 5 ng/ml TGF- β after 96 hours compared to untreated control (A). Representative microscopic images and quantification showing the effect of RLX (125, 250, 500, 1000 ng/ml) on the migration of hPSCs after 7 hours incubation (B). Data represents mean \pm SEM for at least 3 independent experiments. Statistical differences are * p <0.05, ** p <0.01, *** p <0.001

3.3 Preparation and characterization of RLX-SPION conjugates

After confirming the pharmacological effects of RLX *in vitro*, we conjugated it to SPION (~60 nm) using carbodiimide reaction, as illustrated in a schematic representation in Fig. 4A. The successful conjugation of RLX to SPION was confirmed by a dot blot analysis using anti-RLX antibody, followed by Prussian blue iron staining to detect iron oxide nanoparticles. Fig. 4B shows the qualitative representation of RLX (column 1), RLX-SPION (column 2), SPION alone (column 3) and supernatant (column 4) of the left and right blots. In the left blot, absence of RLX expression in SPION alone and supernatant suggests no binding of anti-RLX to SPION and no unconjugated RLX was found after the reaction, respectively. Quantitative analysis of Prussian blue staining in the right blot in RLX and RLX-

SPION indicates the successful conjugation with a yield of about 91.23%. Dynamic light scattering (DLS) shows a slight increase in the hydrodynamic size of SPION after conjugation with RLX (Fig. 4C, 4E). Next, we observed an increase of negative surface charges (zeta potential) of the particles after RLX conjugation (Fig. 3D, 3E), indicating a successful conjugation with no major alterations in the physicochemical properties of the nanoparticles.

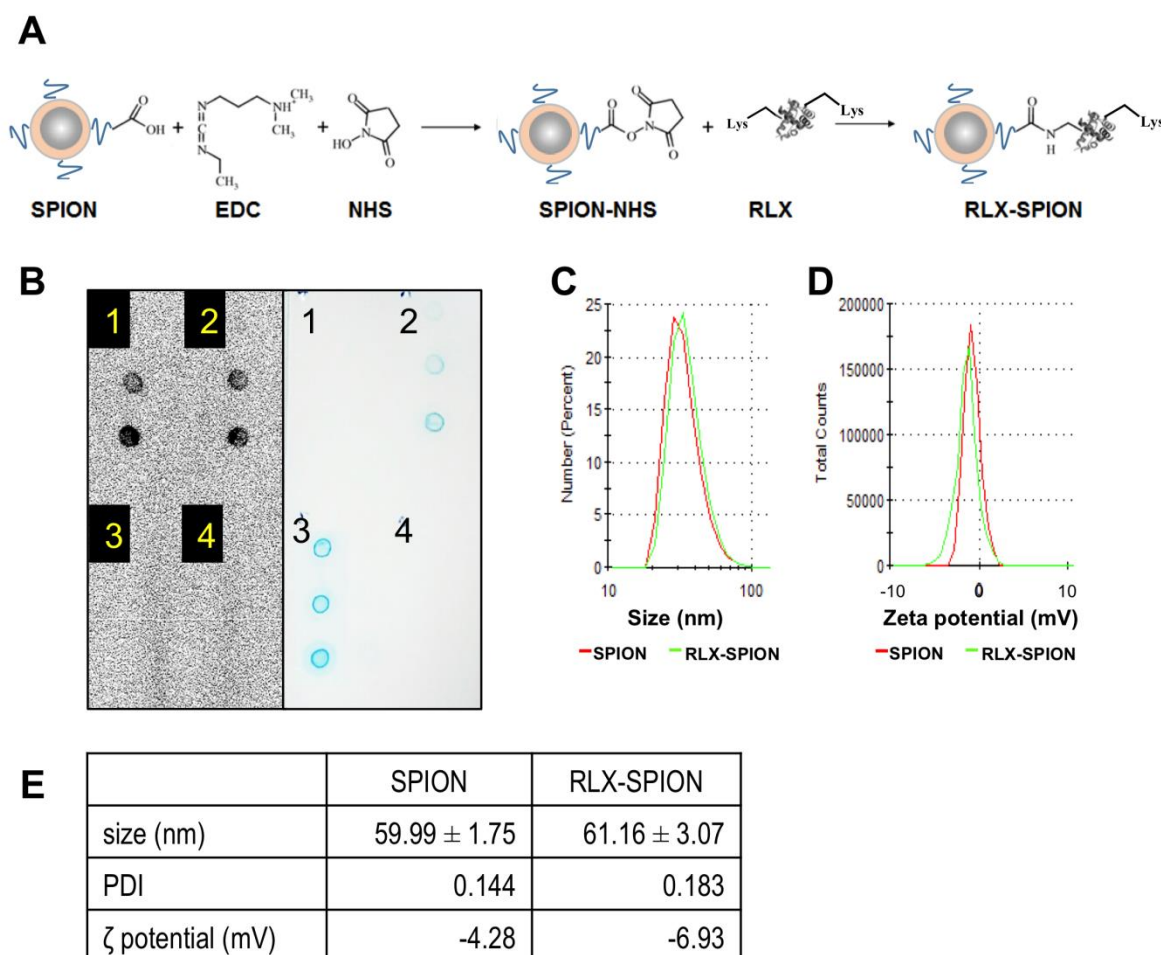


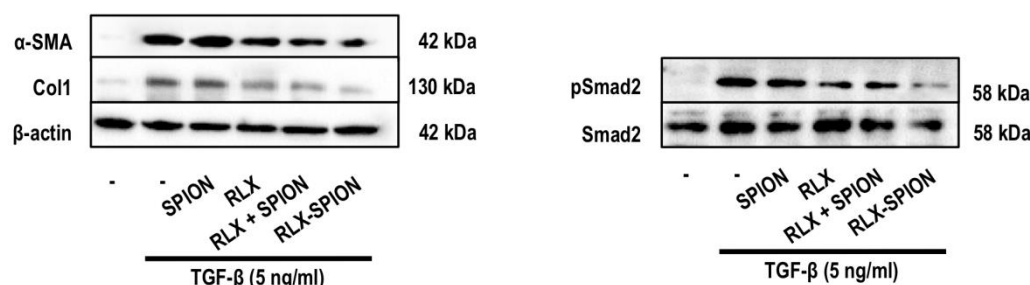
Figure 4. Conjugation of RLX to superparamagnetic iron oxide nanoparticles (SPION). (A) Schematic representation of conjugation of RLX to SPION using carbodiimide chemistry. (B) Immunoblot (left panel) of RLX (1), RLX-SPION (2), SPION (3), and supernatant of the reaction (4) and iron staining (right panel) of each sample as mentioned previously. Images show the presence of RLX and SPION suggesting successful conjugation. Histograms of dynamic light scattering (C), zeta potential (D), and detailed physicochemical data (E) for SPION, RLX-SPION, .

3.4 RLX-SPION inhibits hPSC differentiation into CAF like myofibroblasts

Since the conjugation of RLX to SPION could hinder its biological activity, we examined the effect of RLX-SPION in hPSCs in comparison with free RLX. As a control, we also examined the effect of SPION alone and the effect of mixture of SPION and RLX (unconjugated). The presence of SPION did not affect hPSCs activity *in vitro* (Fig. 5A-B). Surprisingly, we found that RLX-SPION was more

effective in inhibiting hPSCs activation compared to free RLX. As shown in Fig. 5A, the western blot analysis confirmed that reduction in α -SMA expression was much higher with RLX-SPION compared to free RLX. We furthermore demonstrated that the reductions in α -SMA and collagen-1 were due to the inhibition of TGF- β signaling, as confirmed by the inhibition of Smad2 phosphorylation (Fig. 5B).

A



B

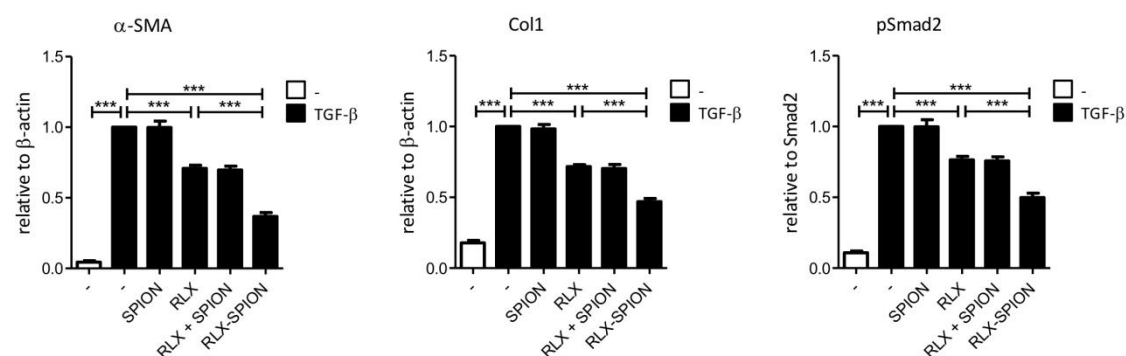


Figure 5. Effect of RLX-SPION on TGF- β mediated hPSCs differentiation. Western blots (A) and quantification (B) showing increased inhibitory effect of RLX-SPION compared to free RLX on the protein expression of α -SMA and Col-1 in hPSCs treated with 5 ng/ml TGF- β for 24 hours and on the phosphorylation of Smad2 in hPSCs treated with 5 ng/ml TGF- β for 1 hour. Data represents mean \pm SEM for at least 3 independent experiments. Statistical differences are ** $p < 0.01$, *** $p < 0.001$

Next, we examined the effect of RLX-SPION on the contractility and migration of hPSCs. We found that RLX-SPION also significantly inhibited the TGF β -induced contraction in collagen gel assay and hPSC migration in scratch (wound healing) assays (Fig. 6A and 6B). These effects were higher than free RLX, which might be due to multivalent effect of RLX on SPION.

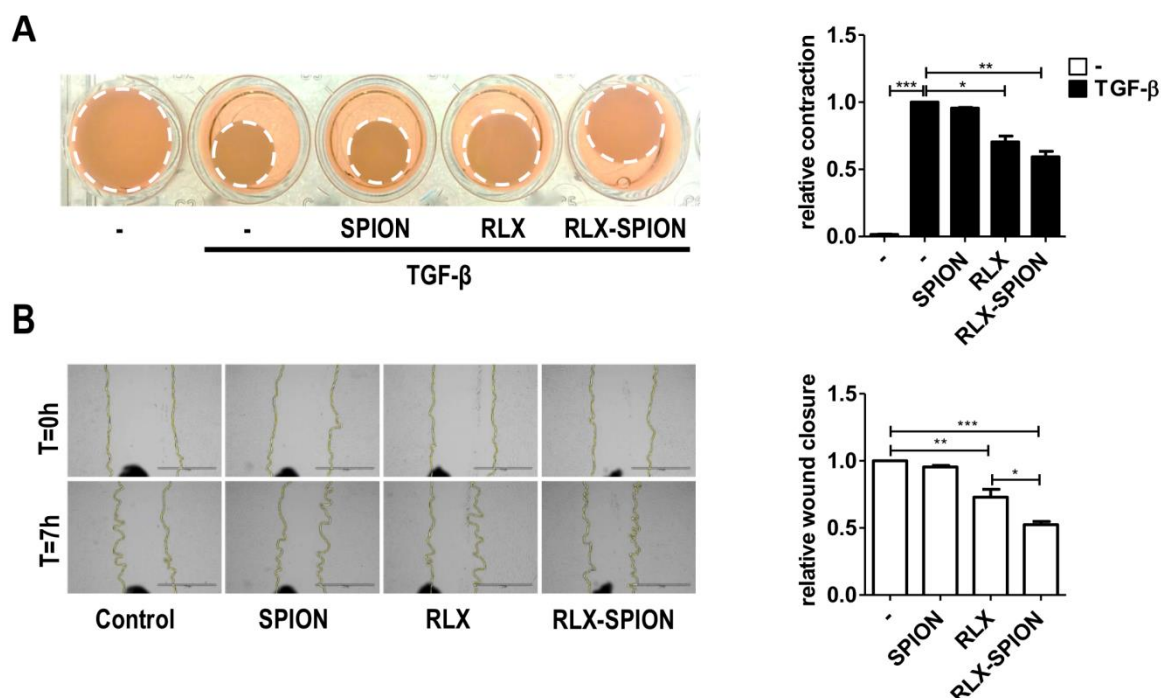


Figure 6. Effect of RLX-SPION on hPSCs contractility and migration. (A) Representative images and quantification showing increased inhibition of TGF- β induced hPSCs contraction after 96 hours incubation with RLX-SPION compared to free RLX. (B) Representative microscopic images and quantification showing increased inhibition of hPSCs migration after 7 hours incubation with RLX-SPION compared to free RLX. Data represents mean \pm SEM for at least 3 independent experiments. Statistical differences are * $p < 0.05$, ** $p < 0.01$, *** $p < 0.001$

3.5 RLX inhibits the tumor growth and potentiates the effect of gemcitabine in co-injection pancreatic tumor xenograft model

Next, we investigated whether RLX-SPION is able to inhibit the differentiation of hPSC into CAF-like myofibroblasts *in vivo* and thereby diminish the tumor-promoting effects i.e. tumor growth, fibrosis and barrier for chemotherapy. To achieve this, we first established a stroma-rich pancreatic tumor xenograft model by co-injecting PANC-1 tumor cells and hPSCs into the flank of immuno-deficient mice (Fig. 6A). We confirmed that these tumors generate abundant tumor stroma and induce CAF markers, thereby mimic human pancreatic tumor to study the effect on tumor stroma (data not shown). After the tumors were established, we administered intravenous injections of vehicle, RLX or RLX-SPION (equivalent to 20 μ g/kg RLX) with or without combination of gemcitabine (50 mg/kg, i.p.) twice a week. Treatment with RLX showed an early reduction of tumor growth but then tumors grew again, while RLX-SPION showed much higher tumor inhibitory effects (Fig. 7B). Interestingly, both RLX alone and RLX-SPION strongly induced the anti-tumor effect of gemcitabine (Fig. 7B and 7C). Importantly, only RLX-SPION showed a significantly increased the effect of gemcitabine (Fig. 7C). None of the treatments showed any negative effect on the body weight (Fig. 7D).

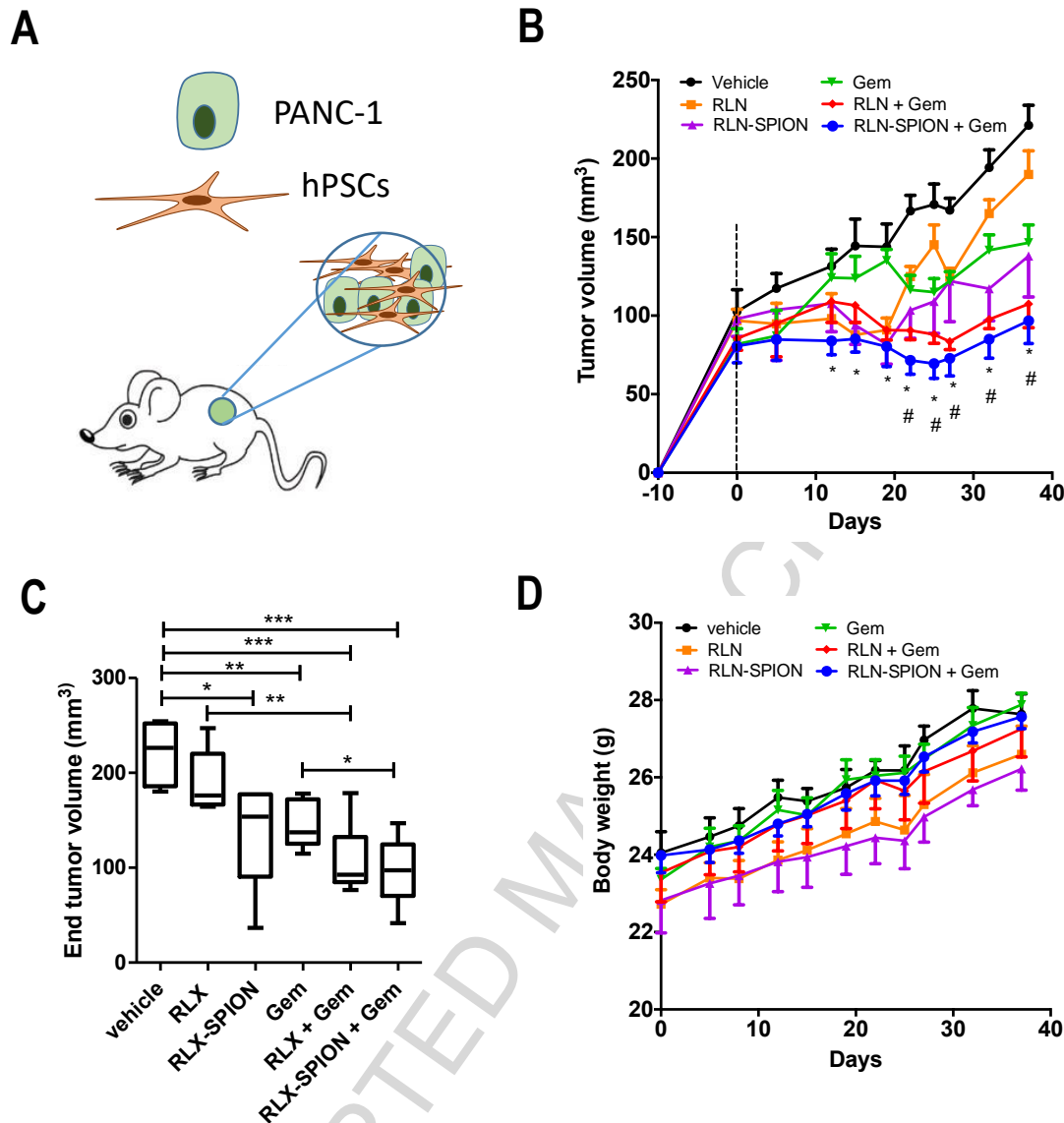


Figure 7. Effect of RLX and RLX-SPION treatment on in vivo tumor growth. (A) Schematic representation of the co-injection of Panc-1 and hPSCs subcutaneous tumor model. The effect of RLX and RLX-SPION co-treatment with gemcitabine on the tumor growth (B) of co-injection (Panc1 and hPSCs) subcutaneous xenografts in mice, * $p < 0.05$ versus vehicle group and # $p < 0.05$ versus Gem group and tumor volumes at the end time point (C) the differences are * $p < 0.05$, ** $p < 0.01$, *** $p < 0.001$. The effect of RLX and RLX-SPION cotreatment with gemcitabine on the body weight of co-injection (Panc1 and hPSCs) subcutaneous tumor bearing mice (D). $N = 5-6$ mice per group.

Furthermore, we analyzed the isolated tumors for the effect on the hPSC activation (desmin as a CAF marker), fibrosis (collagen-1 accumulation) and vasculature (CD31 as endothelial marker) using immunohistochemical staining (Fig. 8A-C). These data showed that RLX-SPION treated mice had a significant reduction of these marker compared to untreated tumors, while RLX showed only a minor but not significant reductions (Fig. 8A-C). Furthermore, these effects were irrespective of the gemcitabine treatment, indicating the actual effect of targeted RLX. These data indicate that targeting of RLX using SPION could strongly inhibit CAF formation in vivo and thereby diminish hPSC-induced

collagen deposition and tumor growth. Collagen is a barrier for drug delivery and reduction of collagen caused by RLX-SPION led to the improved therapeutic efficacy.

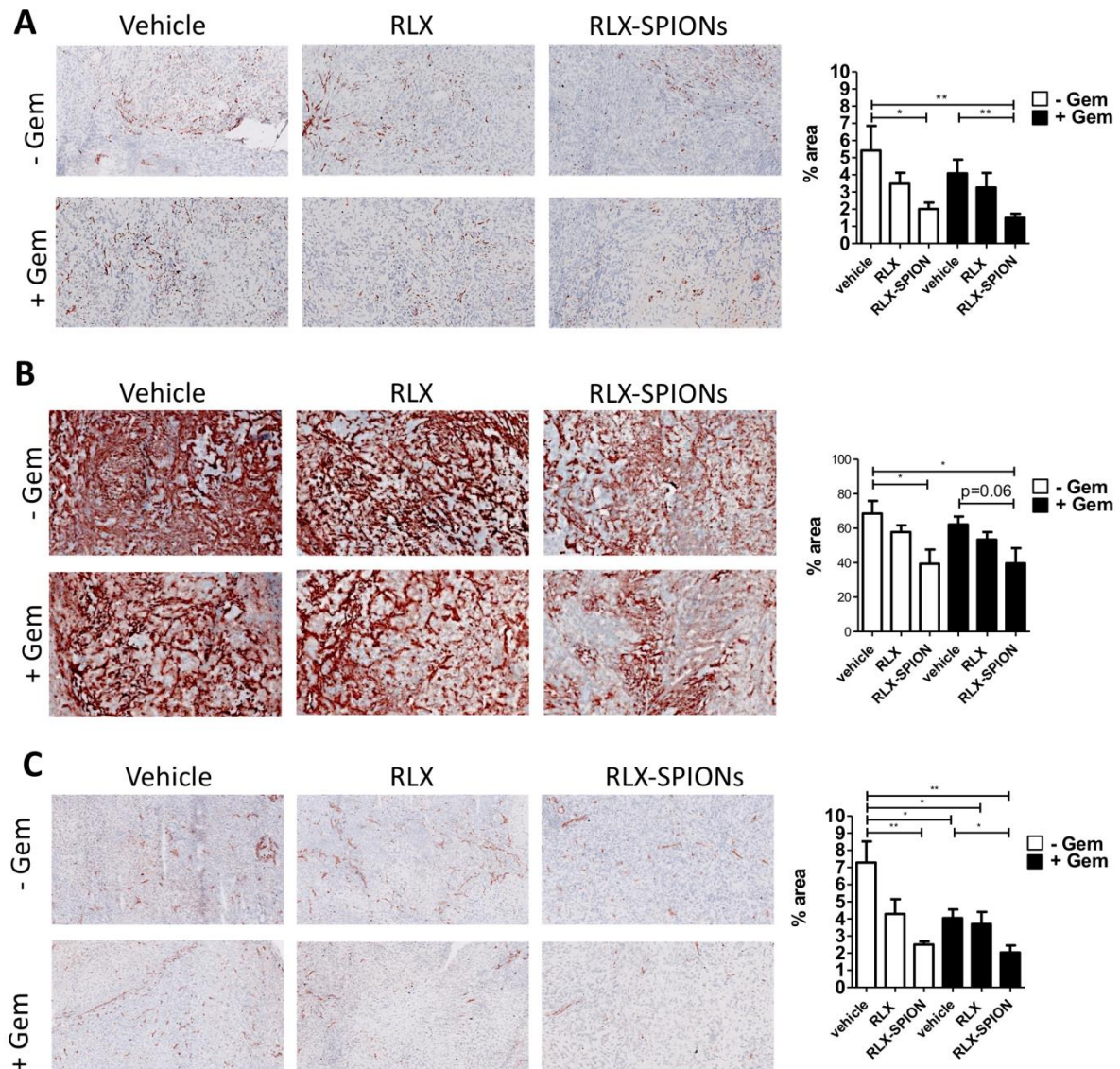


Figure 8. Effect of RLX and RLX-SPION treatment on expression of Panc1+hPSCs tumor xenografts in mice. Immunohistochemistry and quantification of staining for CAF marker desmin (A), ECM protein Collagen-1 (B), and endothelial marker CD31 (C) in tumors treated with RLX and RLX-SPION with or without Gemcitabine. Scale bar 300 μ m. Data represents mean \pm SEM for $n=5-6$ mice per group. Statistical differences are $*p<0.05$, $**p<0.01$.

4. Discussion

In this study, we for the first time demonstrate that targeting of an endogenous peptide hormone RLX using SPION inhibits hPSC-induced fibrosis and tumor growth as well as potentiate the effect of gemcitabine in pancreatic cancer. Desmoplastic reaction in tumor or so-called tumor stroma plays an important role in tumor growth and progression as well as acts as a barrier to chemotherapy [6–8]. Tumor stroma in pancreatic tumor can account for up to 90% of the total tumor mass [6,29]. In the

present study, RLX inhibited hPSCs differentiation into CAF-like myofibroblasts and ECM production by intervening TGF- β signaling pathway. By conjugating RLX to SPION, greater inhibitory effects were gained compared to free RLX. *In vivo* in a stroma-rich mouse tumor model, RLX-SPION showed anti-tumor effects by inhibiting hPSC-induced tumor growth and also enhanced the effect of gemcitabine.

Human PSCs are believed as the main source of CAFs in tumor stroma of pancreatic cancer [9,11,30,31]. The differentiation of hPSCs into CAF-like myofibroblasts is induced by cytokines such as TGF- β as a result of the crosstalk with cancer cells and other stromal cells in the tumor microenvironment. RLX, a peptide hormone, has been shown to be efficacious in inhibiting/reversing fibrosis in cardiac and renal fibrosis models [18–22]. A study reported a comparable approach in addressing pancreatic cancer by employing adenovirus expressing relaxin [32]. In the present study, we performed different approach of combination therapy by targeting relaxin. We showed that TGF- β -activated hPSCs overexpressed RLX-specific surface receptor, RXFP1 and treatment with RLX resulted in reduced TGF β -induced hPSCs differentiation *in vitro*. In literature, RLX has been shown to inhibit the TGF- β -mediated activation of cardiac and renal fibroblasts [18–22]. The ECM secretion and contractility are key features of activated hPSCs to generate dense tumor stroma and enhance intratumoral tension, which inhibit tumor drug penetration [33]. Studies have shown that reduction of fibrosis is able to enhance the therapeutic efficacy of chemotherapy [34,35]. Interestingly, in the present study treatment with RLX reduced both TGF- β -induced collagen production and contraction which shows its ability to inhibit key stromal features in relation to stromal barrier. hPSCs are known to migrate in the tumor microenvironment and support tumor metastasis. In this study, treatment with RLX also reduced the migration of hPSCs, indicating a strong effectivity of RLX.

Biologics such as peptides and proteins are susceptible for enzymatic degradation and are also rapidly cleared from the body. To protect them from the degradation and prolong their half-life, various types of nanocarriers are commonly used [36]. Likewise, in this study, we used SPION to overcome the drawbacks of RLX such as rapid degradation and short circulation. The advantage of SPION is multifold including small size (known for evading reticuloendothelial system and better tumor penetration) [37,38], large surface area allowing surface conjugation and detection using MRI [39]. Since RLX needs to bind to the RXFP1 receptor, a membranous receptor present on hPSCs, we conjugated RLX on the surface of SPION with a PEG spacer allowing RLX to bind freely to the receptor. Studies showed SPION do not elicit cytokine response and is considered non-toxic at low dose [40–42]. It is crucial to notice that after conjugation such a molecule can lose its activity due to conjugation at the receptor interaction site or steric hindrance caused by the conjugation. RLX is comprised of chain A and B joint with a linker chain. In literature, chain A has been shown to be responsible for the bioactivity [43,44], while the chain B seems to be required for proper confirmation. We found that chain B had 2 lysine groups and a N-terminal amine group, which we likely used for conjugating RLX to SPION using carbodiimide chemistry. This conjugation strategy allowed chain A available for binding to the receptor without the release of RLX from SPION. Our *in vitro* effect studies confirmed that RLX-SPION did not lose the activity, however, surprisingly the conjugated form resulted in greater activity compared to free RLX. This might be due to increased stability allowing longer duration of action and/or confinement of the molecules allowing better interaction with the receptor. In

addition, it is known that multivalent interaction instead of monovalent interaction can result in stronger and more selective interaction [45]. Therefore, multivalency of RLX in RLX-SPION might have contributed to the enhanced effects.

In line with the *in vitro* data, administration of RLX-SPION into co-injected (Panc-1 and hPSC) human tumor-bearing mice reduced the activation of hPSCs, as indicated by the reduced desmin expression levels. Since the activated hPSCs are responsible for ECM production and inducing angiogenesis, inhibition of hPSC activation led to the reduction of both ECM deposition and angiogenesis, as indicated by the decreased expression of collagen-1 and CD31 in tumor stroma, respectively. In contrast, free RLX did not show any significant reduction, highlighting the benefit of targeting. We have earlier shown that hPSCs induce tumor growth after combining with PANC-1 tumor cells *in vivo*, demonstrating that hPSCs contribute to the tumor growth [46]. In this study, the inhibition of hPSC activation by RLX-SPION resulted into slower tumor growth. In addition, when combined with gemcitabine, RLX-SPION significantly induced the effect of gemcitabine which is attributed to reduced collagen deposition, allowing better drug penetration. In contrast, free RLX did not significantly improve the effect of gemcitabine, which is in line of the lack of effect of RLX on collagen deposition.

In conclusion, this study demonstrates that the delivery of RLX using SPION is an attractive approach to enhance the therapeutic efficacy of RLX *in vivo*. Inhibition of hPSCs activation by RLX-SPION not only inhibited the collagen deposition and angiogenesis, but also retarded the tumor growth. Moreover, RLX-SPION induced the anti-tumor effect of gemcitabine by reducing collagen deposition, a main barrier for limiting tumor drug delivery. Furthermore, detection of SPION using MRI might be used for detecting tumor delivery. Altogether, this study presents a novel nanotherapeutic approach for impaing the effect of tumor stroma to achieve an effective treatment against pancreatic tumor.

Financial supports

The study was funded by The Indonesian Endowment Fund for Education (LPDP), Indonesia and University of Twente.

Conflicts of interest

The authors have no other relevant affiliations or financial involvement with any organization or entity with a financial interest in or financial conflict with the subject matter or materials discussed in the manuscript apart from those disclosed. J.P. is the founder and stakeholder of the ScarTec Therapeutics BV.

6. References

- [1] R.L. Siegel, K.D. Miller, A. Jemal, Cancer statistics, 2018, CA. Cancer J. Clin. 68 (2018) 7–30. doi:10.3322/caac.21442.
- [2] D.P. Ryan, T.S. Hong, N. Bardeesy, Pancreatic Adenocarcinoma, N. Engl. J. Med. 371 (2014) 1039–1049. doi:10.1056/NEJMra1404198.
- [3] L.A. Bliss, E.R. Witkowski, C.J. Yang, J.F. Tseng, Outcomes in operative management of pancreatic cancer, J. Surg. Oncol. 110 (2014) 592–598. doi:10.1002/jso.23744.
- [4] T. Conroy, F. Desseigne, M. Ychou, O. Bouché, R. Guimbaud, Y. Bécouarn, A. Adenis, J.-L. Raoul, S. Gourgou-Bourgade, C. de la Fouchardière, J. Bennouna, J.-B. Bachet, F. Khemissa-Akouz, D. Péré-Vergé, C. Delbaldo, E. Assenat, B. Chauffert, P. Michel, C. Montoto-Grillot, M.

- Ducieux, G.T.D. of U. and the P. Intergroup, FOLFIRINOX versus Gemcitabine for Metastatic Pancreatic Cancer, *Nejm*. 364 (2011) 1817–1825. doi:10.1056/NEJMc1107627#SA1.
- [5] D.D. Von Hoff, T. Ervin, F.P. Arena, E.G. Chiorean, J. Infante, M. Moore, T. Seay, S.A. Tjulandin, W.W. Ma, M.N. Saleh, M. Harris, M. Reni, S. Dowden, D. Laheru, N. Bahary, R.K. Ramanathan, J. Tabernero, M. Hidalgo, D. Goldstein, E. Van Cutsem, X. Wei, J. Iglesias, M.F. Renschler, Increased Survival in Pancreatic Cancer with nab-Paclitaxel plus Gemcitabine, *N. Engl. J. Med.* 369 (2013) 1691–1703. doi:10.1056/NEJMoa1304369.
- [6] D. Xie, K. Xie, *HHS Public Access*, 2 (2016) 133–143. doi:10.1016/j.gendis.2015.01.002.Pancreatic.
- [7] L. Miao, C.M. Lin, L. Huang, Stromal barriers and strategies for the delivery of nanomedicine to desmoplastic tumors, *J. Control. Release*. 219 (2015) 192–204. doi:10.1016/j.jconrel.2015.08.017.
- [8] J. Prakash, Cancer-Associated Fibroblasts: Perspectives in Cancer Therapy, *Trends in Cancer*. 2 (2016) 277–279. doi:10.1016/j.trecan.2016.04.005.
- [9] H. Li, X. Fan, J. Houghton, Tumor microenvironment: The role of the tumor stroma in cancer, *J. Cell. Biochem.* 101 (2007) 805–815. doi:10.1002/jcb.21159.
- [10] M.H. Sherman, R.T. Yu, D.D. Engle, N. Ding, A.R. Atkins, H. Tiriach, E.A. Collisson, F. Connor, T. Van Dyke, S. Kozlov, P. Martin, T.W. Tseng, D.W. Dawson, T.R. Donahue, A. Masamune, T. Shimosegawa, M. V. Apte, J.S. Wilson, B. Ng, S.L. Lau, J.E. Gunton, G.M. Wahl, T. Hunter, J.A. Drebin, P.J. O'Dwyer, C. Liddle, D.A. Tuveson, M. Downes, R.M. Evans, Vitamin D receptor-mediated stromal reprogramming suppresses pancreatitis and enhances pancreatic cancer therapy, *Cell*. 159 (2014) 80–93. doi:10.1016/j.cell.2014.08.007.
- [11] P.P. Provenzano, C. Cuevas, A.E. Chang, V.K. Goel, D.D. Von Hoff, S.R. Hingorani, Enzymatic Targeting of the Stroma Ablates Physical Barriers to Treatment of Pancreatic Ductal Adenocarcinoma, *Cancer Cell*. 21 (2012) 418–429. doi:10.1016/j.ccr.2012.01.007.
- [12] A. Allam, A.R. Thomsen, M. Gothwal, D. Saha, J. Maurer, T.B. Brunner, Pancreatic stellate cells in pancreatic cancer: In focus, *Pancreatology*. 17 (2017) 514–522. doi:10.1016/j.pan.2017.05.390.
- [13] S.P. Pothula, Z. Xu, D. Goldstein, R.C. Pirola, J.S. Wilson, M. V. Apte, Key role of pancreatic stellate cells in pancreatic cancer, *Cancer Lett.* 381 (2016) 194–200. doi:10.1016/j.canlet.2015.10.035.
- [14] J. Schnittert, M.A. Heinrich, P.R. Kuninty, G. Storm, J. Prakash, Reprogramming tumor stroma using an endogenous lipid lipoxin A4 to treat pancreatic cancer, *Cancer Lett.* 420 (2018) 247–258. doi:10.1016/j.canlet.2018.01.072.
- [15] R.A.D. Bathgate, M.L. Halls, E.T. van der Westhuizen, G.E. Callander, M. Kocan, R.J. Summers, Relaxin Family Peptides and Their Receptors, *Physiol. Rev.* 93 (2013) 405–480. doi:10.1152/physrev.00001.2012.
- [16] F. Hisaw, Experimental relaxation of the pubic ligament of the guinea pig, *Proc Soc Exp Biol Med*. 23 (1926) 661–663.
- [17] A.H. MacLennan, The role of the hormone relaxin in human reproduction and pelvic girdle relaxation, *Scand J Rheumatol.* 88 (1991) 7–15.
- [18] B.L. Henry, B. Gabris, Q. Li, B. Martin, M. Giannini, A. Parikh, D. Patel, J. Haney, D.S. Schwartzman, S.G. Shroff, G. Salama, Relaxin suppresses atrial fibrillation in aged rats by reversing fibrosis and upregulating Na⁺ channels, *Hear. Rhythm*. 13 (2016) 983–991. doi:10.1016/j.hrthm.2015.12.030.
- [19] C.S. Samuel, E.N. Unemori, I. Mookerjee, R.A.D. Bathgate, S.L. Layfield, J. Mak, G.W. Tregear, X.J. Du, Relaxin modulates cardiac fibroblast proliferation, differentiation, and collagen production and reverses cardiac fibrosis in vivo, *Endocrinology*. 145 (2004) 4125–4133. doi:10.1210/en.2004-0209.
- [20] Y.P. Wang, P. Wang, L. Dong, H. Chen, Y.Q. Wu, H.W. Li, M. Li, Relaxin Inhibit Cardiac Fibrosis Induced by Phorbol 12-myristate 13-acetate Letter to the Editor, *Biomed Env. Sci.* 27 (2014) 138–141. doi:10.3967/bes2014.030.
- [21] C.S. Samuel, H. Bodaragama, J.Y. Chew, R.E. Widdop, S.G. Royce, T.D. Hewitson, Serelaxin is a more efficacious antifibrotic than enalapril in an experimental model of heart disease, Hypertension. 64 (2014) 315–322. doi:10.1161/HYPERTENSIONAHA.114.03594.
- [22] B.M. Huuskens, A.F. Wise, A.J. Cox, E.X. Lim, N.L. Payne, D.J. Kelly, C.S. Samuel, S.D. Ricardo, Combination therapy of mesenchymal stem cells and serelaxin effectively attenuates renal fibrosis in obstructive nephropathy, *FASEB J.* 29 (2015) 540–553. doi:10.1096/fj.14-254789.
- [23] D. Peer, J.M. Karp, S. Hong, O.C. Farokhzad, R. Margalit, R. Langer, Nanocarriers as an emerging platform for cancer therapy, *Nat. Nanotechnol.* 2 (2007) 751–760. doi:10.1038/nnano.2007.387.

- [24] V. Wagner, A. Dullaart, A.K. Bock, A. Zweck, The emerging nanomedicine landscape, *Nat. Biotechnol.* 24 (2006) 1211–1217. doi:10.1038/nbt1006-1211.
- [25] P.B. Santhosh, N.P. Ulrih, Multifunctional superparamagnetic iron oxide nanoparticles: Promising tools in cancer theranostics, *Cancer Lett.* 336 (2013) 8–17. doi:10.1016/j.canlet.2013.04.032.
- [26] F. Dilnawaz, A. Singh, C. Mohanty, S.K. Sahoo, Dual drug loaded superparamagnetic iron oxide nanoparticles for targeted cancer therapy, *Biomaterials.* 31 (2010) 3694–3706. doi:10.1016/j.biomaterials.2010.01.057.
- [27] M. Zhao, M.F. Kircher, L. Josephson, R. Weissleder, Differential Conjugation of Tat Peptide to Superparamagnetic Nanoparticles and Its Effect on Cellular Uptake, (2002) 840–844. doi:10.1021/bc0255236.
- [28] R. Bansal, E. Post, J.H. Proost, A. De Jager-Krikken, K. Poelstra, J. Prakash, PEGylation improves pharmacokinetic profile, liver uptake and efficacy of Interferon gamma in liver fibrosis, *J. Control. Release.* 154 (2011) 233–240. doi:10.1016/j.jconrel.2011.05.027.
- [29] A. Neesse, P. Michl, K.K. Frese, C. Feig, N. Cook, M.A. Jacobetz, M.P. Lolkema, M. Buchholz, K.P. Olive, T.M. Gress, D.A. Tuveson, Stromal biology and therapy in pancreatic cancer, *Gut.* 60 (2011) 861–868. doi:10.1136/gut.2010.226092.
- [30] M.A. Shields, S. Dangi-Garimella, A.J. Redig, H.G. Munshi, Biochemical role of the collagen-rich tumour microenvironment in pancreatic cancer progression, *Biochem. J.* 441 (2012) 541–552. doi:10.1042/BJ20111240.
- [31] P.R. Kuninty, J. Schnittert, G. Storm, J. Prakash, MicroRNA Targeting to Modulate Tumor Microenvironment, *Front. Oncol.* 6 (2016) 1–8. doi:10.3389/fonc.2016.00003.
- [32] K.H. Jung, I.K. Choi, H.S. Lee, H.H. Yan, M.K. Son, H.M. Ahn, J.W. Hong, C.O. Yun, S.S. Hong, Oncolytic adenovirus expressing relaxin (YDC002) enhances therapeutic efficacy of gemcitabine against pancreatic cancer, *Cancer Lett.* 396 (2017) 155–166. doi:10.1016/j.canlet.2017.03.009.
- [33] R.K. Jain, Normalizing tumor microenvironment to treat cancer: Bench to bedside to biomarkers, *J. Clin. Oncol.* 31 (2013) 2205–2218. doi:10.1200/JCO.2012.46.3653.
- [34] C. Polydorou, F. Mpekris, P. Papageorgis, C. Voutouri, T. Stylianopoulos, Pirfenidone normalizes the tumor microenvironment to improve chemotherapy, *Oncotarget.* 8 (2017) 24506–24517. doi:10.18632/oncotarget.15534.
- [35] F. Mpekris, P. Papageorgis, C. Polydorou, C. Voutouri, M. Kalli, A.P. Pirentis, T. Stylianopoulos, Sonic-hedgehog pathway inhibition normalizes desmoplastic tumor microenvironment to improve chemo- and nanotherapy, *J. Control. Release.* 261 (2017) 105–112. doi:10.1016/j.jconrel.2017.06.022.
- [36] R. Solaro, F. Chiellini, A. Battisti, Targeted Delivery of Protein Drugs by Nanocarriers, 2010. doi:10.3390/ma3031928.
- [37] M.R. Dreher, W. Liu, C.R. Michelich, M.W. Dewhirst, F. Yuan, A. Chilkoti, Tumor vascular permeability, accumulation, and penetration of macromolecular drug carriers, *J. Natl. Cancer Inst.* 98 (2006) 335–344. doi:10.1093/jnci/djj070.
- [38] Z. Popović, W. Liu, V. Chauhan, A nanoparticle size series for in vivo fluorescence imaging, *Angew.* 49 (2010) 8649–8652. doi:10.1002/anie.201003142.A.
- [39] M. Mahmoudi, S. Sant, B. Wang, S. Laurent, T. Sen, Superparamagnetic iron oxide nanoparticles (SPIONs): Development, surface modification and applications in chemotherapy, *Adv. Drug Deliv. Rev.* 63 (2011) 24–46. doi:10.1016/j.addr.2010.05.006.
- [40] Q. Feng, Y. Liu, J. Huang, K. Chen, J. Huang, K. Xiao, Uptake, distribution, clearance, and toxicity of iron oxide nanoparticles with different sizes and coatings, *Sci. Rep.* 8 (2018) 1–13. doi:10.1038/s41598-018-19628-z.
- [41] E.A. Vermeij, M.I. Koenders, M.B. Bennink, L.A. Crowe, L. Maurizi, J.P. Vallée, H. Hofmann, W.B. Van Den Berg, P.L.E.M. Van Lent, F.A.J. Van De Loo, The in-vivo use of superparamagnetic iron oxide nanoparticles to detect inflammation elicits a cytokine response but does not aggravate experimental arthritis, *PLoS One.* 10 (2015) 1–15. doi:10.1371/journal.pone.0126687.
- [42] R. Weissleder, D. Stark, B. Engelstad, B. Bacon, C. Compton, D. White, P. Jacobs, J. Lewis, Superparamagnetic iron oxide: pharmacokinetics and toxicity, *Am. J. Roentgenol.* 152 (1989) 167–173. doi:10.2214/ajr.152.1.167.
- [43] M.A. Hossain, J.D. Wade, R.A.D. Bathgate, Chimeric relaxin peptides highlight the role of the A-chain in the function of H2 relaxin, *Peptides.* 35 (2012) 102–106. doi:10.1016/j.peptides.2012.02.021.
- [44] M.A. Hossain, K.J. Rosengren, C.S. Samuel, F. Shabanpoor, L.J. Chan, R.A.D. Bathgate, J.D. Wade, The minimal active structure of human relaxin-2, *J. Biol. Chem.* 286 (2011) 37555–37565. doi:10.1074/jbc.M111.282194.

- [45] J. Voskuhl, U. Kauscher, B.J. Ravoo, Multivalent molecular recognition on the surface of bilayer vesicles, in: *Multivalency Concepts, Res. Appl.*, 2018: pp. 177–204.
- [46] C. Strell, K.J. Norberg, A. Mezheyeuski, J. Schnittert, P.R. Kuninty, C.F. Moro, J. Paulsson, N.A. Schultz, D. Calatayud, J.M. Löhr, O. Frings, C.S. Verbeke, R.L. Heuchel, J. Prakash, J.S. Johansen, A. Östman, Stroma-regulated HMGA2 is an independent prognostic marker in PDAC and AAC, *Br. J. Cancer*. 117 (2017) 65–77. doi:10.1038/bjc.2017.140.

Graphical abstract

ACCEPTED MANUSCRIPT